A&A 430, 435–442 (2005)
DOI: 10.1051/0004-6361:20041801

Astronomy & Astrophysics

X-ray to UV variability correlation in MCG–6-30-15

P. Arévalo[1], I. Papadakis[2], B. Kuhlbrodt[3,4], and W. Brinkmann[1]

[1] Max-Planck-Institut für extraterrestrische Physik, Postfach 1312, 85741 Garching, Germany
e-mail: parevalo@mpe.mpg.de
[2] Department of Physics, University of Crete, PO Box 2208, 71 003 Heraklion, Crete, Greece
[3] Astrophysikalisches Intitut Potsdam, An der Sternwarte 16, 14482 Potsdam, Germany
[4] Hamburger Sternwarte, Gojenbergsweg 112, 21029 Hamburg, Germany

Received 5 August 2004 / Accepted 22 September 2004

Abstract. We used a ∼300 ks long *XMM-Newton* observation of the Seyfert 1 galaxy MCG–6-30-15 to study the correlation between the 0.2–10 keV X-ray and the 3000–4000 Å U bands. We found a significant correlation peak at a time lag of $\tau_{\rm max} \sim$ 160 ks where the UV flux variations preceded the variations in the X-ray band. We interpret this result as evidence in favour of Comptonisation models where the observed X-rays are produced through Compton up-scattering of thermal UV seed photons from an accretion disc, as this process naturally predicts the UV variations to precede similar flux variations in the X-rays. The length of the time lag favours models where the observed UV and the seed-photon-emitting regions are connected by perturbations of the accretion flow traveling inwards through the disc, affecting first the main U-band-emitting radii and then the innermost region where the bulk of the seed photons is expected to be produced. Finally, the absence of significant features in the correlation function with X-ray flux variations preceding those in the UV indicates that the observed U-band photons are not mainly produced through reprocessing of hard X-rays in this source.

Key words. accretion, accretion disks – galaxies: active – galaxies: individual: MCG–6-30-15 – X-rays: individual: MCG–6-30-15

1. Introduction

The spectral energy distributions of Active Galactic Nuclei (AGNs) are extremely broad, often ranging from radio wavelengths up to gamma rays. Though this is well established, the origin of the emission is still a matter of debate. In general most of the AGN's luminosity is in the so called Big Blue Bump in the optical-UV regime, and a considerable fraction of the energy is emitted in the X-ray band. The study of the variability of the sources in these energy bands and their correlations can provide important information on the emission mechanisms.

The most widely accepted model for the energy release in AGN is accretion of matter onto a supermassive black hole, and the accretion flow is thought to form an optically thick disc. In the standard picture this accretion disc radiates thermally mainly in the optical/UV band, for AGN black hole masses of $\sim 10^6$–10^8 $M_\odot$. The production of X-rays is commonly attributed to Compton up-scattering of UV-photons (e.g. Sunyaev & Titarchuck 1980) by hot electrons in a corona (Haardt & Maraschi 1991). Under this hypothesis the UV and X-ray light curves are expected to be correlated with the X-rays lagging the UV. However, it is also possible that the X-rays produced this way would illuminate the disc or other surrounding optically thick material and produce UV radiation through reprocessing (e.g. Guilbert & Rees 1988). If the bulk of the observed UV continuum arises from this thermal re-emission the resulting light curves would again be correlated but this time the UV should lag the X-rays. Some models where the UV and X-ray emission come from a single continuum process predict no time lags between the bands. In principle simultaneous observations of these two energy bands with good time resolution and sampling should provide information about the physical and geometrical conditions of the emission region and help to discriminate between the models.

Several multi-wavelength monitoring campaigns of AGN conducted in the previous decade aimed to search for correlations between X-rays and optical/UV emission. A definite correlation could be found in only a few cases and the sign or existence of a time lag differed from case to case (see Maoz et al. 2002, for the puzzling results of their long-duration campaign of NGC3516 together with a summary of previous studies). The existence of positive as well as negative time lags suggests that different processes could be dominating the emission at different times and, in general, does not imply any simple relation between the energy bands. Some cases where no lags were found might be explained in terms of inappropriate sampling of the light curves, if the time lags are for example much shorter that the typical spacing between data points.

In this paper we study the temporal variations of the Seyfert 1 galaxy MCG–6-30-15 ($m_B \sim 13.8$, $z = 0.00775$).

This galaxy is famous for its broad and skewed Fe K_α line (Tanaka et al. 1995), which is consistent with fluorescent emission from a disc close to the central supermassive black hole. This spectral feature is strong evidence for the accreting black hole model and limits the primary hard X-ray emitting region to a few Schwarzschild radii R_S (Fabian & Vaughan 2003). MCG–6-30-15 has been extensively observed in X-rays where it shows large and rapid flux variability (see eg. Iwasawa et al. 1996; Fabian et al. 2003). Timing analyses indicate a featureless, red-noise-like power density spectrum with a possible break at 10^{-4} Hz as its only characteristic time scale (Vaughan et al. 2003).

The aim of the work presented here is to determine the relationship between the UV and X-ray light curves of MCG–6-30-15. The results of cross-correlation analyses of the variability of the light curves are compared with the predictions of different emission models to estimate their applicability to this object. We make use of simultaneous X-ray and UV data obtained with the instruments on board *XMM-Newton* . The observation spans approximately 430 ks (i.e. ∼5 days) and the time resolution, limited by the sampling time of the UV light curves, is ∼1.2 ks. Therefore we can use these data to search for correlations between the X-ray and UV light curves on time scales of a few ks with lags up to a few days.

The paper is organized as follows: in Sect. 2 we describe the data reduction and the construction of the light curves. Section 3 contains the cross correlation analysis, implications of the results are discussed in Sect. 4 and we summarize our conclusions in Sect. 5.

2. Data reduction and light curves

MCG–6-30-15 was observed with *XMM-Newton* between July 31st and August 5th 2001, during revolutions 301, 302 and 303. The observations spanned a total time of ∼430 ks with 80 ks, 122 ks and 123 ks stretches of scientifically useful, uninterrupted exposures. For the analysis we used data from the EPIC-PN detector (Strüder et al. 2001) to construct the X-ray light curve and from the Optical Monitor, OM (Mason et al. 2003), for the UV.

The X-ray data used here have already been analyzed extensively by several authors. Vaughan et al. (2003) studied in detail the time variability of the X-ray continuum in the PN energy band. The broad Fe K_α line in the spectrum has been studied and modeled by Fabian et al. (2002), Fabian & Vaughan (2003), Miniutti et al. (2003) and Ballantyne et al. (2003) using this same data set. Vaughan & Fabian (2004) tested different spectral models for the PN 3–10 keV band, and the soft X-ray spectrum was studied by Turner et al. (2003, 2004) using the reflection grating spectrometer (RGS) data of the same observation.

2.1. X-ray light curves

All EPIC-PN exposures were taken in the small-window (SW) mode using the medium filter. We processed the data using XMMSAS version 5.4.1. The light curve was constructed following the procedure described in Fabian et al. (2002), differing only in extraction radius (30″ in the previous analysis, 50″ in the present work). This bigger radius was chosen to include at least 90% of the energy of a point source (Ghizzardi & Molendi 2001) and results in a slightly higher count rate (6% difference) than that presented in the work mentioned above.

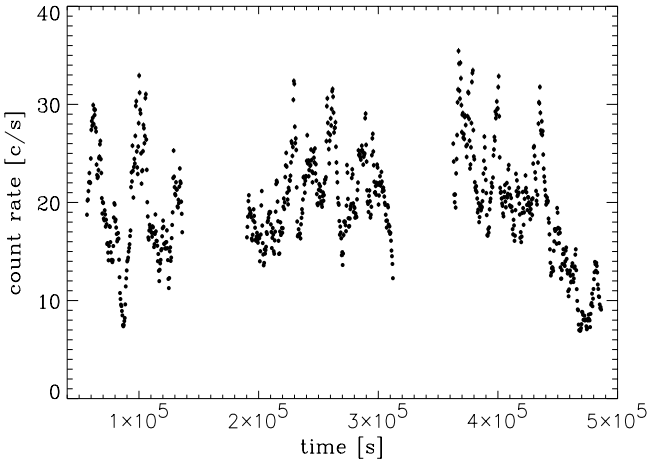

Fig. 1. X-ray light curve from the PN data in 400 s bins. Time is in seconds starting from 0:00:00 h of July 31st, 2001. The errors in the count rate are typically smaller than the symbols.

The background-subtracted light curves were binned in different bin sizes and the corresponding errors were calculated by propagating the Poissonian noise. Bins with data gaps were corrected for their effective exposure times. Since all exposures were taken in the same observation mode we did not correct for mode-dependent exposure time losses such as dead time or out-of-time events.

In general the background activity was low, on average less than 1% of the source count rate. Only in the last few ks of each exposure did the background increase significantly. These segments of the light curves were excluded from the analyses. The final light curve is shown in Fig. 1.

The X-ray light curve displays large amplitude variations in all observable time scales with an overall maximum-to-minimum ratio of ∼5. The power spectrum of this light curve has approximately a broken power-law shape and the frequency of the break at $\sim 10^{-4}$ Hz indicates the presence of a characteristic time scale at $\sim 10^4$ s in the system. The average luminosity of the source in the 0.2–10.0 keV band is $\sim 10^{43}$ erg/s and the minimum-to-maximum luminosity difference has a value of $\Delta L \sim 1.5 \times 10^{43}$ erg/s (Vaughan et al. 2003).

2.2. UV light curves

The OM is a 30 cm optical/UV telescope co-aligned with the X-ray telescopes on board *XMM-Newton* . It is sensitive in the 1600–6000 Å wavelength range and its typical point spread function has a full width at half maximum of 2.2″ in the *U* band. For this observation the OM was operated in imaging mode using the *U* filter (3000–4000 Å). We processed the data using the task OMICHAIN of XMMSAS version 5.4.1. The data consist of a sequence of 274 snapshot exposures 800 s long typically separated by time gaps of 320 s. Figure 2 shows

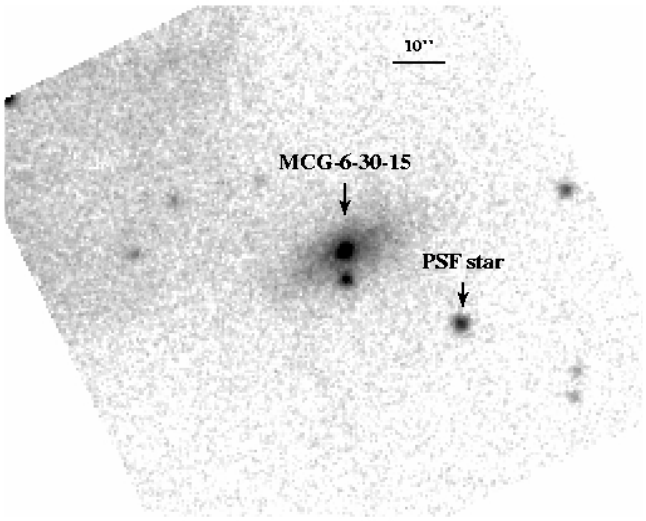

Fig. 2. OM image of MCG–6-30-15. The host galaxy is clearly seen around the brightest point source, which corresponds to the AGN. The secondary object 6″ to the south of the nucleus and the non-uniform background pattern were taken into account in the fitting procedure.

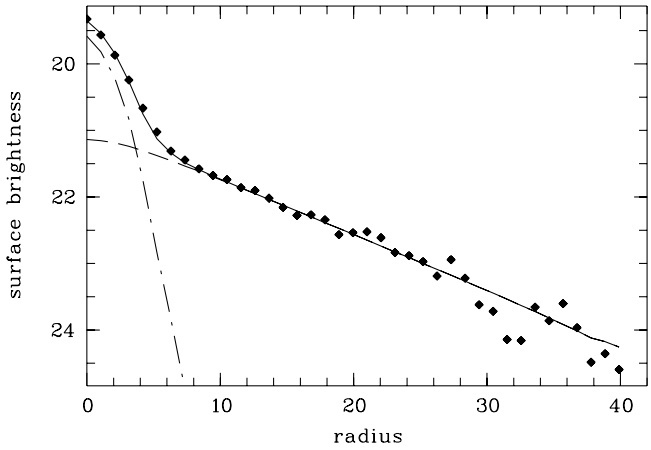

Fig. 3. Light profile fit with a two-component model. The radius is in pixels (1 pixel = 0.48″) and the surface brightness in arbitrary units. The solid line shows the total model fit to the data (filled diamonds). The dashed line shows the disc contribution, and the dashed-dotted line the nuclear component.

one of the OM exposures on logarithmic scale. The U-band luminosity of the AGN is smaller than that of the total host galaxy so the Poissonian error in the total (galaxy+nucleus) counts introduces a significant scatter that may mask the intrinsic variability of the nucleus. It was therefore essential to separate the contribution of the nucleus from that of the rest of the galaxy to obtain an accurate measure of the AGN variability. To do this we used the algorithm developed by Kuhlbrodt et al. (2004) which decomposes the image of a galaxy into disc, bulge and/or nuclear point source components.

The principle behind the algorithm is that the light distribution of the nucleus is modeled with the image of a nearby star. Since both the star and the active nuclear region are not resolved in the UV, their images are representative of the point-spread function (PSF) of the optical system. Spatial or temporal variation of the PSF do not play a role in our case: as a nearby star with high signal-to-noise was always present in the images, variations in the PSF were taken into account by determining its actual shape in every exposure. This star, labeled PSF star in Fig. 2, is only used for the PSF modeling and not for photometric comparison. The model of the galaxy consists of the exponential disk profile by Freeman (1970) and a de Vaucouleurs (1948) profile for the bulge, expanded to two dimensions with elliptical isophotes (see Kuhlbrodt et al. 2004 for details) and convolved with the PSF. The nuclear and galaxy components are then fitted simultaneously.

2.2.1. Image decomposition

As a first approach MCG–6-30-15 was fitted using a three-component model accounting for a disc, a bulge and a nuclear point source. The bulge contribution to the galaxy flux is small, typically ∼10% of the disc flux. This component was subsequently discarded from the fitting procedure to improve the accuracy in the determination of the nuclear flux.

As can be seen in Fig. 3 the two-component (disc+nuclear point source) model is a good approximation and fits the light profile accurately. This figure shows the model fit, where the dashed line represents the disc, the dashed-dotted line the nuclear component and the solid line represents the sum of the components fitted to the data points (filled diamonds). It is important to note that although MCG–6-30-15 has been classified as an E/S0 galaxy based on the galaxy morphology as seen in the optical band, in the U band it is very well fitted by a Freeman disc model only.

We used the two-component model to fit all 274 images individually, allowing only for variable nucleus and disc normalisations. The disc fluxes obtained showed a very small scatter in their values, entirely accountable for by Poissonian noise, and gave no indication of strong systematic changes in the photometric performance of the detector. However, as the nuclear flux is small compared to the disk flux, $F_{\rm nuc}/F_{\rm disc} \sim 0.17$, and the simultaneous determination of both fluxes is slightly degenerate, even small errors in the disc flux could result in significant artificial variations in the nuclear light curve. To make sure that the nuclear variability present in the light curve was not an artifact of this degeneracy we modified the routine in order to enforce a constant disc flux. This was done by taking the average disc flux to produce a galaxy template and compare this to the galaxy component in each image, excluding the central region. The background level was then fine-tuned to minimize their difference. By following this procedure we could subtract the background accurately and fix the disc flux to the template value. The final nuclear flux was determined by fitting once more the nuclear component to all the background-corrected images.

To estimate the error in the determination of the nuclear flux we made dedicated Monte Carlo simulations using synthetic images. We generated images with the template-galaxy disc parameters and appropriate PSFs for the nuclear component. We used 10 different disc-to-nucleus flux ratios around the measured values. Observational noise was then added

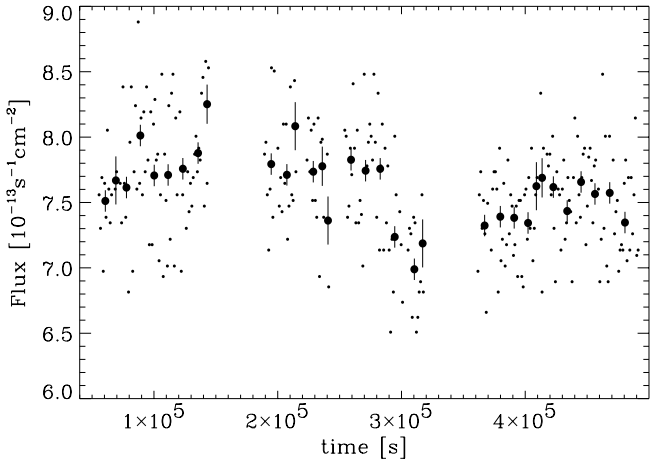

Fig. 4. U-band light curve; dots show the unbinned data and filled circles the 10-ks-binned light curve. For clarity, only the error bars of the binned light curve are shown. The errors were calculated using Monte Carlo simulations as described in the text. The time is in seconds, counted from 0:00:00 h, July 31st, 2001.

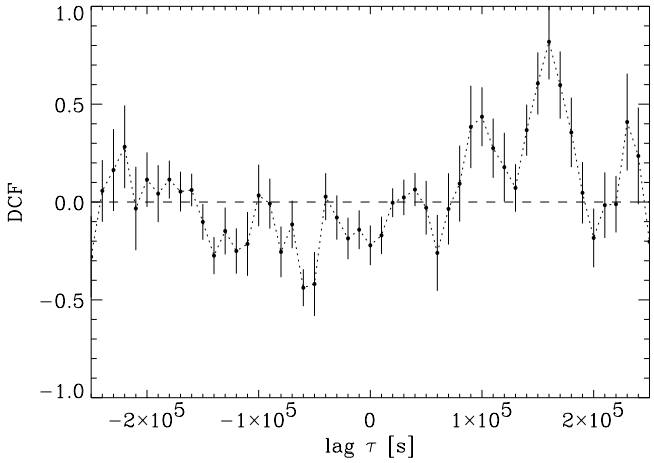

Fig. 5. Discrete Correlation Function (DCF) calculated between the full X-ray band (0.2–10 keV) and the UV light curve as a function of time lag in seconds. Positive lags imply UV leading X-rays. The DCF binning used is 10 ks. The error bars plotted represent the standard error of the DCF only and do not account for the effects of the correlations between nearby data points.

before running the fitting routine on the synthetic data set. We ran the process for 170 synthetic images to estimate the performance of the decomposition routine in the specific conditions of the data. The errors in the determination of the nuclear flux were 3.5%, independent of the flux ratio in the range studied.

The light curve was constructed by plotting the nuclear flux as a function of the midpoint time of each exposure and is shown in Fig. 4. To reduce the scatter produced partly by observational noise we binned the data in 10 ks (∼10 exposures per bin) and calculated the errors by averaging quadratically the errors of the individual points within the corresponding bin. In this way the intrinsic low amplitude variability of the light curve becomes evident; it can be seen as the filled circles overlaid on the same plot. The binned UV light curve varies smoothly on time scales of ∼100 ks with a maximum amplitude variation of 15% throughout the observation, small compared with the variations by a factor of 5 observed in the X-rays. The average U-band nuclear flux measured is $\sim 7.60 \times 10^{-13}$ erg/s/cm^2. Assuming a distance of 30 Mpc (Hayashida et al. 1998) and galactic extinction of $A_\lambda = 0.334$ (Schlegel et al. 1998), the average nuclear luminosity in the U band is $\sim 1 \times 10^{41}$ erg/s. For comparison we also constructed the light curve of the star used for PSF modeling using simple aperture photometry. The resulting 10-ks-binned light curve showed small fluctuations, a χ^2 test gave a value of $\chi^2_{\rm red} = 1.34$ for 35 degees of freedom against the constant flux hypothesis. These fluctuations are somewhat larger than those expected purely from Poissonian noise and could reflect variations in the sensitivity of the detector. However, given their small amplitude these variations could only account for a fraction of the fluctuations seen in the nuclear light curve which gives a value of $\chi^2_{\rm red} = 6.89$ for the same test.

3. Cross-correlation analysis

The cross correlation between the UV and X-ray light curves was computed using the discrete correlation function (DCF) method of Edelson & Krolik (1988). The X-ray data were binned in 5 ks bins to smooth out the rapid variations, which are not observed in the UV. The UV light curve was binned averaging five consecutive points to reduce the scatter and the error of the individual points. The DCF between the full X-ray band (0.2–10 keV) and the UV light curve using a lag bin of size $\Delta\tau = 10$ ks is plotted in Fig. 5. The most significant feature is the positive correlation peak at $\tau_{\rm max} = 160$ ks with amplitude $DCF_{\rm max} = 0.82$ where the variations in the UV lead those in the X-rays. No significant peaks, either positive or negative, are evident in negative lags i.e. there is no indication of UV variations being driven by changes in the X-ray flux on the time scales probed.

In order to estimate the error on $\tau_{\rm max}$ and $DCF_{\rm max}$ we used the Monte Carlo method described by Peterson et al. (1998). We find $\tau = 160^{+45}_{-65}$ ks, while $DCF_{\rm max} = 0.82^{+0.17}_{-0.25}$ where the errors represent the 95% confidence limits. These errors are associated mainly with the uncertainties caused by the observational sampling of the light curves and the flux uncertainty in the individual measurements. However, since both light curves are probably realisations of a red-noise process, it is possible to detect significant correlations even if they are intrinsically uncorrelated. In order to investigate this issue further, we performed a second numerical experiment.

As already mentioned in Sect. 2.1, the X-ray power spectrum has a broken power-law shape. Vaughan et al. (2003) found a slope of −1 up to a frequency of 10^{-4} Hz above which the slope steepens to a value of ∼−2 for one of their fitted models. Assuming this power spectral shape, we used the method of Timmer & König (1995) to construct 10 000 synthetic light curves with a mean and variance equal to those of the 0.2–10 keV light curve. The points in the synthetic light curves were sampled every 10 s in order to account for aliasing effects, while the length was 10 times larger than that of the observed X-ray light curve in order to account for red-noise leak. These synthetic light curves were then re-binned in 5 ks bins

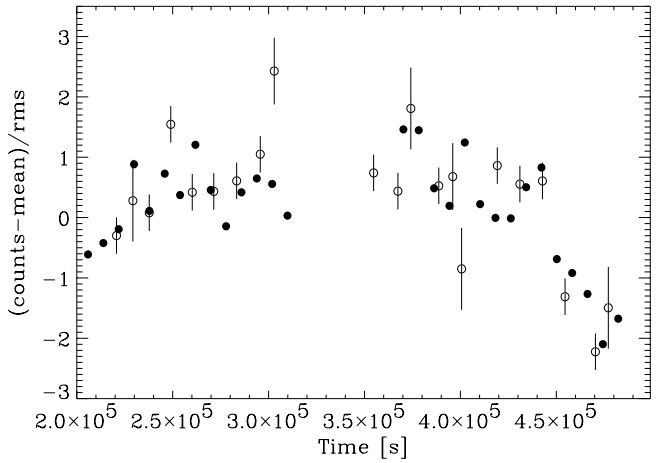

Fig. 6. Overlap region of the normalized UV light curve (open circles) in 10 ks bins and back-shifted X-ray light curve (filled circles) in 8 ks bins. The X-ray light curve was shifted back in time by 160 ks. The X-ray error bars are smaller than the symbols.

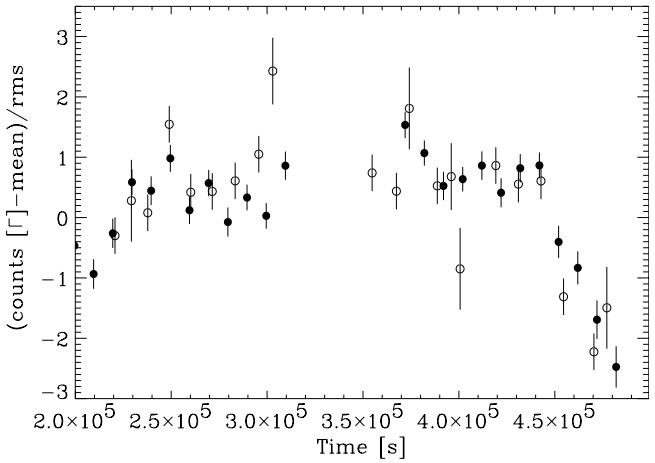

Fig. 7. *U*-band light curve in 10 ks bins (open circles) overlaid on the photon-index curve of the hard X-ray spectrum fitted with a power-law model (filled circles). The photon-index (Γ) curve has been back-shifted by the 160 ks corresponding to the highest peak in the DCF between softness ratio and *U*-band light curves. Both curves were mean-subtracted and divided by their rms.

and sampled to match the length and sampling pattern of the original X-ray light curve. We estimated the DCF between the observed UV light curve and each of the synthetic light curves, registering the resulting $DCF_{\max}$. Only in 1.5% of all cases did we find a $DCF_{\max}$ value larger than 0.82, at any lag. We repeated this procedure using slightly flatter and steeper power spectrum slopes with nearly identical results. We conclude that the positive correlation that we detect in Fig. 5 is significant in the sense that most probably it is due to an intrinsic coupling between the observed UV and X-ray flux variations. In the same simulations we found peaks with $|DCF_{\max}| > 0.4$ in approximately 90% of the cases indicating that the peaks seen at $\tau \sim -60$, 100 and 230 ks are not significant.

Figure 6 shows a plot of the X-ray and UV light curves normalized to their mean (filled and open circles, respectively). The X-ray light curve is back-shifted by 160 ks and the plot shows the period where the light curves overlap. The light curves are binned in order to eliminate the fast, large amplitude variations of the X-ray flux and to increase the signal-to-noise ratio in the case of the UV. This figure reveals clearly the reason for the large DCF peak value at lag 160 ks. If we take into account the delay, the modulation of the UV flux matches well that of the smoothed X-ray light curve over the interval sampled. The correlation suggests an intrinsic link between the observed variations in the two energy bands on time scales of ∼10–100 ks, which operates with a delay of ∼160 ks.

We also investigated briefly the correlation between the UV and the X-ray light curves in different energy bands. The resulting DCFs are very similar to that shown in Fig. 5, as is expected since the different X-ray energy bands show similar variations. In all cases, we observe a strong peak at lag ∼ 160 ks, although its amplitude shows minor differences. We find that the 2–4 keV and 8–10 keV light curves are the best correlated with the UV, both with a value of $DCF_{\max} = 0.84$. The 4–7-keV-band light curve, which is representative of the Fe K_α line emission, shows a marginally weaker correlation ($DCF_{\max} = 0.83$), while the soft-excess-component (0.2–1.0 keV) light curve shows the weakest correlation with the UV light curve with a peak of $DCF_{\max} = 0.78$.

3.1. DCF between the UV flux and the variations in the X-ray energy spectrum

In order to investigate possible correlations between the UV flux and the variations in the X-ray energy spectrum we used the 2–4 and 8–10 keV light curve to construct the 2–4 keV/8–10 keV softness ratio curve. These energy bands were selected to show the spectral changes in the 2–10 keV continuum while minimizing the contribution of the Fe line and the soft excess. The softness ratio so defined is representative of the slope of the continuum, where higher values correspond to steeper spectra. We used softness ratio and UV light curves in 5 ks bins and lag bin size of $\Delta\tau = 10$ ks to calculate the DCF, and found a moderately good correlation ($DCF_{\max} = 0.67$) again at a time lag of ∼160 ks. We should point out that this value of the $DCF_{\max}$ is found in approximately 10% of the Monte Carlo trials described above and so the correlation is formally not significant on its own.

The X-ray spectrum in these energy bands can be well fitted by a power-law model, with photon index $\Gamma \sim 2.0$. To investigate the behaviour of the spectral slope we fitted a power-law model to the 2–4 and 8–10 keV bands every 10 ks. Figure 7 shows a plot of the UV light curve (open circles) and of the photon-index (Γ) curve normalized to their mean, where the photon-index curve has been back-shifted by 160 ks. Like in Fig. 6 we show only the period where the UV flux and the Γ curves overlap. The figure shows that the UV flux is well correlated with the X-ray spectral slope, the 2–10 keV continuum flattens (i.e. Γ decreases) as the UV flux decreases, with a time delay of 160 ks.

4. Discussion

The connection between the UV and X-ray emission from AGN is thought to be primarily due to two processes: Comptonisation of UV photons into X-rays and reprocessing of X-rays into the UV range. Here we discuss both mechanisms and confront their predictions with our results.

4.1. Comptonisation scenario

The positive peak found in the DCF with UV variations leading those in the X-rays suggest that variations in the thermal component (accretion disc) drive the changes in the emission of the scatterer (corona) on time scales ≥10 ks, and constitutes evidence for the Comptonisation scenario.

4.1.1. Origin of the time lag

To investigate the possible origin of the time lag we estimate the physical separation of the emitting regions. The X-ray emission region is thought to be compact and located very close to the black hole due to its rapid high-amplitude variability and by the spectral shape of the fluorescent Fe line. Fabian et al. (2003) limit the size of the hard X-ray source to a few R_S. The U-band emission is probably produced thermally through viscous dissipation in the accretion disc. We use the standard thin disc model to estimate the radii of maximum U-flux emission. For this we assume a disc radial temperature profile given by $T_{\rm eff}(R) = [(3GM\dot{M}/8\pi\sigma R^3)(1 - \sqrt{R_{\rm in}/R})]^{1/4}$ where M is the black hole mass, $\dot{M}$ is the accretion rate estimated from the bolometric luminosity, σ is the Stefan-Boltzmann constant, R is the radius in the disc and $R_{\rm in}$ is the radius of the inner edge of the disc (see eg. Kato et al. 1998). We consider the disc to be composed of rings of approximately uniform temperature radiating locally as black bodies. For a black hole mass between 10^6 and 10^7 $M_\odot$ (Hayashida et al. 1998; Czerny et al. 2001; Vaughan et al. 2003) and bolometric luminosity of 7×10^{43} erg/s (Czerny et al. 2001) the rings producing the largest flux in the U band (3000–4000 Å) are at $R \sim 100\,R_S$ for a 10^6 $M_\odot$ black hole and $R \sim 25\,R_S$ for a 10^7 $M_\odot$ black hole. The radii obtained correspond to light travel times between the emitting regions of only a few ks, too short to explain the measured lag.

However, if the accretion disc indeed extends down to a few R_S as the shape of the Fe line suggests, most of the disc flux should be emitted in this small radius and mainly in higher energy photons than the observed 3000–4000 Å band. Therefore the bulk of the seed photons for Comptonisation may be emitted in a different region of the accretion disc than the observed U band photons. The length of the time lag that we observe favours models where variations in the accretion flow affect first the flux at outer radii and then in the innermost region. In this case, the observed delay would correspond to the time needed for the accretion flow fluctuations to travel inwards from the radius where most of the U band photons are produced (∼25−100 R_S) to the innermost region of ∼5 R_S where most of the seed photons for Comptonisation are emitted. As a reference time scale, the sound crossing time in a standard thin disc between these radii with black hole mass of 10^6 $M_\odot$ is ∼1000 ks, marginally consistent with the measured lag. If we consider that the variable part of the UV light curve might arise from radii smaller than that producing most of the U band luminosity we obtain shorter sound crossing times, closer to the 160 ks lag. Alternatively, MHD effects might transport perturbations through the accretion disc faster than sound waves and remain a plausible source for the measured lag.

4.1.2. Spectral changes

The Comptonisation scenario is also supported by the correlated variations that we observe between the UV flux and the slope of the X-ray continuum energy spectrum. We find that when the UV flux rises the continuum becomes steeper with a delay of ∼160 ks. This effect is qualitatively consistent with the behaviour of a hot plasma receiving more seed photons, radiating more X-rays and cooling to a new equilibrium temperature, thus producing a steeper power-law spectrum. A similar UV flux/Γ correlation has also been observed in the case of NGC 7469 (Nandra et al. 2000).

We should point out, however, that the UV flux/Γ correlation in MCG–6-30-15 may be merely a by-product of the UV/X-ray flux variability correlation. Figure 8 shows a plot of the best-fitting Γ values as a function of the total count rate in the 2–4 plus 8–10 keV bands. The photon index Γ is well correlated with the count rate, with higher flux corresponding to a steeper spectrum. However, intrinsic Γ variations in MCG–6-30-15 have been questioned in the past using this and other data sets. For example, Taylor et al. (2003) and Fabian & Vaughan (2003) explain the X-ray spectral variations of the source with the combination of two components: a constant slope, variable normalization power-law component and constant reflection component. In this case there are no genuine Γ variations, as the softening of the spectrum is due only to a change in relative normalization of the two fixed shape components. If this is the case then the UV/Γ correlation results merely from the UV/X-ray flux correlation through the good correspondence between X-ray flux and spectral slope. The situation is far from clear, though, as the presence of a constant reflection component may not be able to account for the spectral slope variations of the source as shown by Papadakis et al. (2002). Since we find that both the UV/X-ray-flux light curves and the UV flux/Γ time series are well correlated with the same time delay, the present results do not help to discriminate between the two possibilities.

4.2. Reprocessing scenario

There is observational evidence that the hard X-ray source in this object illuminates cooler nearby material, possibly the accretion disc. The broad and skewed Fe K_α line from fluorescent emission and the reflection hump detected in the X-ray band above 10 keV (Vaughan & Fabian 2004) give support to this statement. It is also expected that the X-rays illuminating such optically thick material would produce UV emission through thermal reprocessing and so produce correlated X-ray and UV

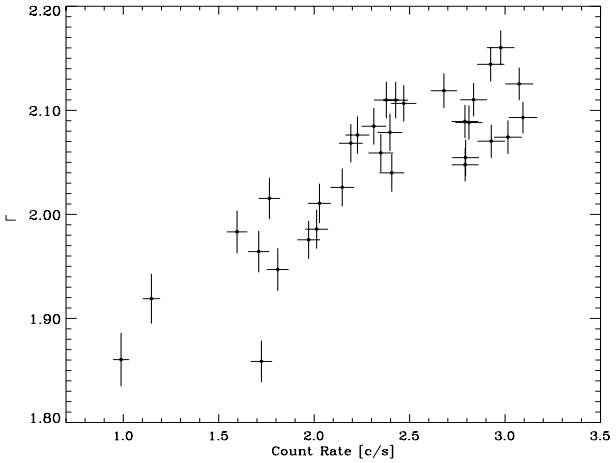

Fig. 8. Photon index Γ of the power-law fitted to the 2–4 keV plus 8–10 keV spectrum as a function of the count rate in these bands.

light curves with X-ray variations leading the UV's. However, the DCF between these light curves showed no positive peaks with negative lags (i.e. with X-rays leading the UV) and so give no indication of reprocessing.

To estimate the amount of reprocessed emission expected from the accretion disc we consider a simple model where the X-rays received by the disc are totally absorbed and re-emitted as black-body radiation. We start by calculating the expected U-band flux emitted by a standard thin disc around a 10^6–10^7 $M_\odot$ black hole with bolometric disc luminosity $L_{\rm bol} = 10^{43.85}$ erg/s (Czerny et al. 2001) through viscous dissipation alone. We obtain the local black-body spectrum of the disc as a function of radius and then integrate the flux in the 3000–4000 Å band from $R = 3\ R_{\rm S}$ to $R = 3000\ R_{\rm S}$. We then recalculate the U-band flux now including the effect of reprocessing. For this simple model we assume that the reprocessed flux adds to the flux from viscous dissipation:

$$F(R) = F_{\rm viscous}(R) + F_{\rm reprocessed}(R)$$
$$= \frac{3GM\dot{M}}{8\pi R^3}\left(1 - \sqrt{\frac{R_{\rm in}}{R}}\right) + \frac{L_{\rm X}\, h}{4\pi(R^2 + h^2)^{3/2}}$$

where R is the radius in the disc and h the height of the X-ray source over the disc. We take the illuminating X-ray flux $L_{\rm X} = 10^{43}$ erg/s and assume the emitting region to be compact, close to the disc axis, and at a height $h = 3 - 10\ R_{\rm S}$. The integrated U-band flux increases by only 3–12% when the illuminating X-ray component is included, where the lower flux results from the smaller height of the X-ray source. More importantly, a change by a factor of 4 in the X-ray flux induces only a change of 4–11% in the total U-band flux for the same range of h values. Considering the simplicity of the model these numbers can only be regarded as reference values. Moreover, they are only upper limits for this geometrical configuration, given that here we assume total reprocessing of the X-ray flux. We conclude that large variations of the X-ray flux can produce variations in the reprocessed component which are too small to be detected in this data, especially if the X-ray source is located at a small height h.

4.3. Comparison with previous results

Several studies of X-ray/UV/Optical correlations in AGN have been carried out in the past. From these only the short-term correlations found can be compared with the work presented here. We have no information on the correlation between the optical/UV and X-rays on long (months/years) time scales for MCG–6-30-15, and the correlated variability properties of other objects appear to depend on the time scales probed. Some objects for which similar studies have been presented are NGC 4051, NGC 7469 and NGC 5548.

Notably Mason et al. (2002) found the 2900 Å UV lagging the 2–10 keV X-ray continuum by 0.2 days from a 1.5 day long *XMM-Newton* observation of NCG 4051. The mass of this object is similar to that of MCG–6-30-15 and the variability amplitudes found for the X-ray and UV bands are comparable with those presented here. However they found a lag of opposite sign and interpret it as evidence for reprocessing, contrary to what we find in MCG–6-30-15. These results might be reconciled by noting that NGC 4051 was observed in a higher-frequency UV band. If the higher-energy UV emission comes from smaller radii of the accretion disc then this band can be affected more strongly by a compact X-ray source close to the centre. In this way the UV-reprocessed component, which is probably present in both objects, would be comparatively stronger in this observation of NGC 4051. A longer (2 month) monitoring of this object gave evidence for X-rays lagging the optical by ∼2.4 days (Shemmer et al. 2003), similar in sign and magnitude to the lag we found in MCG–6-30-15 between X-ray and ∼3500 Å bands.

As mentioned before, Nandra et al. (2000) found a good correlation between UV flux and X-ray spectral index peaking at 0 lag from a 30 day long observation of NGC 7469. This result is similar to what we observe in MCG–6-30-15 considering that a lag of ∼100 ks would not be clearly discernible in their daily binned data. In NGC 5548 Chiang et al. (2000) found the extreme UV (0.1 keV) continuum leading the variations in the soft and hard X-rays by 10 and 40 ks respectively from a 20 day baseline campaign. Again this lag is qualitatively similar to what we find, with lower energies leading the variations of higher energy bands.

On long time scales however the behaviour of the objects studied can be quite different. NCG 5548 shows high-amplitude, highly correlated variability in X-ray and optical bands (Uttley et al. 2003), NGC 3516 also displays high-amplitude variability in both bands but this time the correlation is very weak (Maoz et al. 2002) while NGC 4051 shows very weak optical variability, although well correlated with the much more variable X-rays (Peterson et al. 2000).

It is possible to explain some of the different X-ray/UV long-term correlations observed in different objects by considering the differences in their black-hole masses as noted by Uttley et al. (2003). Since MCG–6-30-15 shows a similar behaviour to both NGC 5548 ($\sim 10^8\ M_\odot$) and NGC 4051 ($\sim 10^6\ M_\odot$) on short time scales, a longer-term optical campaign would be necessary to test the optical variability/black-hole-mass correlation in this object. Apart from this hypothesis it is hard to draw a consistent picture of the behaviour of all the

cases studied given the small number of objects with similar observations and the large number of relevant intrinsic parameters. However, we can note that Uttley et al. (2003), from long-term optical variability amplitude, Shemmer et al. (2003), from considerations of the size of the X-ray-emitting region, and the work presented here, from the magnitude of the observed time lag between X-ray and UV variations, all agree that the connection between these energy bands is probably due to accretion-flow fluctuations traveling inwards across the emission regions.

5. Conclusions

We analyzed simultaneous UV and X-ray data of MCG–6-30-15 to study the relation between the time variability in these two energy bands on time scales of a few ks to a few 100 ks. The X-ray light curve displayed large amplitude variations reaching a maximum-to-minimum count rate ratio of ∼5 which implies a change in luminosity of $\Delta L \sim 10^{43}$ erg/s. The UV light curve was calculated using a sophisticated decomposition technique to determine the nuclear flux accurately against the background of the bright host galaxy. This light curve showed much smaller amplitude variability than the X-rays, not larger than 15% during the whole observation, amounting to $\Delta L < 2 \times 10^{40}$ erg/s.

We found a significant correlation ($DCF_{\max} = 0.82$) between the light curves with a time lag $\tau = 160^{+45}_{-65}$ ks, where the UV variations lead the X-rays. We interpret the sign of this time lag as evidence for models where X-rays arise from Comptonisation of thermal UV photons, as in an accretion disc-corona scenario. The time lag is too long to represent the light travel time from the U-band emitting region of a standard disc to the centre, where the X-rays are thought to be produced. In turn this length favours models where the variations in the disc flux arise from perturbations in the accretion flow traveling inwards through the disc, affecting first the U-band emitting region and then the innermost radii from where the bulk of the seed photons for Comptonisation must come. Finally the cross-correlation analysis gave no significant correlation with negative time lags (ie. with X-ray leading UV) suggesting that the bulk of the observed UV does not arise from reprocessed X-rays.

Acknowledgements. This work is based on observations with *XMM-Newton* , an ESA science mission with instruments and contributions directly funded by ESA Member States and the USA (NASA). We are very grateful to H. Spruit and P. Uttley for useful discussions and to M. Freyberg for OM data-processing assistance. We also thank the anonymous referee for useful comments. P.A. acknowledges support from the International Max Planck Research School on Astrophysics (IMPRS).

References

Ballantyne, D. R., Vaughan, S., & Fabian, A. C. 2003, MNRAS, 342, 239
Czerny, B., Nikolajuk, M., Piasecki, M., & Kuraszkiewicz, J. 2001, MNRAS, 325, 865
Chiang, J., Reynolds, C. S., Blaes, O. M., et al. 2000, ApJ, 528, 292
de Vaucouleurs, G. 1948, Ann. Astrophys., 11, 247
Edelson, R. A., & Krolik, J. H. 1988, ApJ, 333, 646
Fabian, A. C., Vaughan, S., Nandra, K., et al. 2002, MNRAS, 335, L1
Fabian, A. C., & Vaughan, S. 2003, MNRAS, 340, L28
Freeman, K. C. 1970, ApJ, 161, 802
Ghizzardi, S., & Molendi, S. 2001, Proc. Conf. New Visions of the X-ray Universe, ESTEC Nov. 2001
Guilbert, P. W., & Rees, M. J. 1988, MNRAS, 233, 475
Haardt, F., & Maraschi, L. 1991, ApJ, 380, 51
Hayashida, K., Miyamoto, S., Kitamoto, S., Negoro, H., & Inoue, H. 1998, ApJ, 500, 642
Iwasawa, K., Fabian, A. C., Reynolds, C. S., et al. 1996, MNRAS, 282, 1038
Kato, S., Fukue, J., Mineshige, S. 1998, Black-Hole Accretion Disks (Kyoto: Kyoto University Press)
Kuhlbrodt, B., Wisotzki, L., & Jahnke, K. 2004, MNRAS, 349, 1027
Maoz, D., Markowitz, A., Edelson, R., & Nandra, K. 2002, AJ, 124, 1988
Mason, K. O., McHardy I. M., Page M. J. et al. 2002, ApJ, 580, 117
Mason, K. O., Breeveld, A., Much, R., et al. 2001, A&A, 365, 36
Miniutti, G., Fabian, A. C., Goyder, R., & Lasenby, A. N. 2003, MNRAS, 344, 22
Nandra, K., Le, T., George, I. M., Edelson, R. A., et al. 2000, ApJ, 544, 734
Papadakis, I. E., Petrucci, P. O., Maraschi, L., et al. 2002, ApJ, 573, 92
Peterson, B. M., Wanders, I., Horne, K., et al. 1998, PASP, 110, 660
Peterson, B. M., McHardy, I. M., Wilkes, B. J., et al. 2000, ApJ, 542, 161
Schlegel, D., Finkbeiner, D., & Davis, M. 1998, ApJ, 500, 525
Shemmer, O., Uttley, P., Netzer, H., McHardy, I. M. 2003, MNRAS, 343, 1341
Strüder, L., Briel, U. G., Dennerl, K., et al. 2001, A&A, 365, 18
Sunyaev, R., & Titarchuck, L. G. 1980, A&A, 86, 121
Tanaka, Y., Nandra, K., Fabian, A. C., et al. 1995, Nature, 375, 659
Taylor, R., Uttley, P., & McHardy, I. M. 2003, MNRAS, 342, 31
Timmer, J., & König, M. 1995, A&A, 300, 707
Turner, A. K., Fabian, A. C., Vaughan, S., & Lee, J. C. 2003, MNRAS, 346, 833
Turner, A. K., Fabian, A. C., Lee, J., & Vaughan, S. 2004 [arXiv:astro-ph/0405570]
Uttley, P., Edelson, R., McHardy, I. M., et al. 2003, ApJ, 584, 53
Vaughan, S., Fabian, A. C., & Nandra, K. 2003, MNRAS, 339, 1237
Vaughan, S., & Fabian, A. C. 2004, MNRAS, 348, 1415